Journal of Materials Chemistry A

PAPER

View Article Online
View Journal

Spinel MFe_2O_4 (M = Co, Ni) nanoparticles coated on multi-walled carbon nanotubes as electrocatalysts for Li–O_2 batteries†

Cite this: DOI: 10.1039/c4ta00960f

Jiaxin Li,[ab] Mingzhong Zou,[a] Weiwei Wen,[a] Yi Zhao,[bc] Yingbin Lin,[a] Luzhuo Chen,[a] Heng Lai,[a] Lunhui Guan*[bc] and Zhigao Huang*[a]

Received 25th February 2014
Accepted 28th April 2014

DOI: 10.1039/c4ta00960f

www.rsc.org/MaterialsA

Ternary spinel MFe_2O_4 (M = Co, Ni) nanoparticles coated on multi-walled carbon nanotubes (MFe_2O_4/CNTs) were prepared *via* a simple hydrothermal method. Owing to their favorable structures and desirable bi-functional oxygen reduction and evolution activities, the resulting MFe_2O_4/CNT (M = Co, Ni) composites as electrocatalysts for the cathodes deliver better electrochemical performance during the discharge and charge processes compared with that of the pure carbon of ketjen black (KB). The good performance can be attributed to the excellent catalytic activity of highly dispersed MFe_2O_4 (M = Co, Ni) nanoparticles and facile electron transport by supporting CNTs. This preliminary result manifests that the ternary spinel MFe_2O_4/CNT (M = Co, Ni) composites are promising cathode electrocatalysts for non-aqueous Li–O_2 batteries.

1. Introduction

Rechargeable Li–O_2 batteries (LOBs) represent one of the most promising new technologies among the various energy storage systems owing to their very large theoretical gravimetric energy (3505 W h kg^{-1} based on the reversible reaction of $2Li + O_2 \rightarrow Li_2O_2$).[1,2] However, the extremely high energy density of LOBs cannot be fully achieved in practice. In the case of non-aqueous LOBs, the insoluble discharge products of lithium oxides (such as Li_2O_2) deposit in the porous cathode and further block oxygen intake.[3] Consequently, discharge ends quickly when the pores are clogged. The insulating lithium oxides would also lead to a sudden drop of output potential, an increase of charge voltage, and thus loss of round-trip efficiency.[4,5] An effective route to solve this problem is developing highly efficient bi-functional electrocatalysts to decrease the overpotentials for the discharge process (oxygen reduction reaction, ORR), and enhance the charge reaction (oxygen evolution reaction, OER) by reducing the voltage required to dissociate the reaction products.[5,6]

Recently, numerous cathode electrocatalysts have been explored to enhance the LOB performance, including precious metals[7,8] and alloys,[9,10] functional doped-carbon materials,[4,11] metal nitrides[12,13] and metal oxides.[14–19] Among them, the transition metal oxides have attracted extensive attention as alternative electrocatalysts, due to their salient advantages of high catalytic activity, low cost, excellent reliability and environmental friendliness. Typical transition metal oxides such as Co_3O_4,[17] $MnCo_2O_4$,[18] MnO_2[19] and CuO[20] have been reported as effective electrocatalysts for LOBs. For example, typical spinel cobaltite oxides have been investigated as electrocatalysts for the ORR or OER processes.[21] In an oxygen-atom ligand field, Co^{2+} is a high spin ion and substitutionally labile, whereas Co^{3+} with a higher oxidation state is low spin and substitutionally inert.[22,23] The ORR is postulated to take place at active sites associated with the cations at the oxide surface in a higher oxidation state. Dai *et al.* reported a hybrid material of Co_3O_4 nanocrystals grown on reduced graphene oxide as a high-performance bi-functional electrocatalyst for the ORR and OER processes.[24] Furthermore, through substitution of the Ni atom in the spinel lattice, ORR and OER catalytic performance of the resulting $NiCo_2O_4$ composite was further improved. This structure with two solid-state redox couples (*i.e.*, Co^{3+}/Co^{2+} and Ni^{3+}/Ni^{2+}) enables it to exhibit a remarkable catalytic activity.[25,26] Very recently, Chen *et al.* pointed out that the incorporation of Ni cations into the octahedral sites of the spinel crystal structure can improve electrical conductivity and create new active sites with much lower activation energy.[26] These studies inspire us to investigate the electrocatalytic activity of those rarely reported ternary spinel oxides, especially $CoFe_2O_4$ and $NiFe_2O_4$, toward ORR and OER for LOBs.

For further improving the electrocatalyst activities for ORR/OER in LOBs, metal oxides are usually anchored on supporting

[a]College of Physics and Energy, Fujian Normal University, Fuzhou, 350007, China. E-mail: zghuang@fjnu.edu.cn; Fax: +86 591 83832979; Tel: +86 591 83832979

[b]State Key Laboratory of Structural Chemistry, Fujian Institute of Research on the Structure of Matter, Chinese Academy of Sciences, Fuzhou 350002, China. E-mail: guanlh@fjirsm.ac.cn; Fax: +86 591 83792835; Tel: +86 591 83792835

[c]Key Laboratory of Design and Assembly of Functional Nanostructures, Chinese Academy of Sciences, Fuzhou, 350002, China

† Electronic supplementary information (ESI) available. See DOI: 10.1039/c4ta00960f

carbon-based materials including carbon black, carbon nanotubes and graphene.[2,8,18,27] This strategy is expected to offer many advantages, such as (i) the highly conductive carbon affords facile and fast pathways to electrons; (ii) preservation of the initial structure with a high specific surface area directly increases sites for the electrochemical reaction and further increases the capacity of electrochemical storage. Here, ternary spinel MFe_2O_4 (M = Co, Ni) nanoparticles coated on multi-walled carbon nanotubes (MFe_2O_4/CNTs) were prepared *via* a simple hydrothermal method. The electrochemical performance of LOBs with the MFe_2O_4/CNT (M = Co, Ni) composites as electrocatalysts for cathodes was investigated in detail.

2. Experimental

2.1 Synthesis of MFe_2O_4/CNT (M = Co, Ni) composites

The CNTs were purchased from Shenzhen Nanotech Port (Shenzhen, China) and used as received. According to our previous work,[28] 0.075 mmol phenylphosphonic acid and ferric nitrate nonahydrate were dissolved in 10 mL deionized water and sonicated for 10 min to form a homogeneous solution. 3 mg purified CNTs were added and the mixtures were sonicated for 6 h. Then, 0.0375 mmol cobalt(II) acetate tetrahydrate was added to the above solution and sonicated for another 0.5 h. Finally, 200 mg urea was added before the mixture was transferred to a 25 ml Teflon-lined stainless-steel autoclave and kept at 180 °C for 48 h. The $NiFe_2O_4$/CNT composite was synthesized by replacing Co^{2+} with the same mol Ni^{2+}.

2.2 Sample characterization

The structure and morphology of the MFe_2O_4/CNT (M = Co, Ni) composites were characterized by X-ray diffraction (XRD, RIGAKU SCXmini), transmission electron microscopy (TEM, Tecnai G2 F20), energy dispersive X-ray spectroscopy (EDS), and X-ray photoelectron spectroscopy (XPS, VG Scientific ESCALAB MK II).

2.3 Electrochemical measurements

According to our previous report,[29] the electrochemical behaviors were measured in a Swagelok cell with a 0.5 cm^2 hole placed on the cathode side to enable oxygen flow inside. All the batteries were assembled in a dry argon-filled glove box. Working electrodes were prepared by mixing 60 wt% carbon active material (ketjen black, KB), 30 wt% electrocatalysts of MFe_2O_4/CNTs (M = Co, Ni), and 10 wt% polyvinylidene difluoride (PVDF). The loading ratio of the active material is about 1.6–2.0 mg cm^{-2} per electrode. The capacity of LOBs is calculated based on the weight of KB. And then a commercially available electrolyte solution of 1 M LITFSI (lithium bis(trifluoromethanesulfonyl) imide) in TEGDME (tetraethylene glycol dimethyl ether) was impregnated into a glass fiber membrane and sandwiched between a lithium metal anode and an air cathode. The batteries were cycled by LAND 2001A at room temperature with a lower voltage limit of 2.0 V and an upper limit of 4.3 V *versus* Li^+/Li under different conditions after a 2–3 h rest period. The cyclic voltammetry (CV) test was performed on a CHI660D electrochemical workstation at a rate of 0.20 mV s^{-1}. Electrochemical impedance spectra (EIS) were recorded by applying an AC voltage of 5 mV over the frequency range from 1 mHz to 100 kHz.

3. Results and discussion

Fig. 1 shows the XRD pattern of as-synthesized MFe_2O_4/CNT (M = Co, Ni) composites recorded in the range of 2θ from 10° to 80°. As illustrated for $CoFe_2O_4$/CNTs, their diffraction peaks were well indexed to the (111), (220), (311), (222), (400), (422) and (440) planes of cubic $CoFe_2O_4$ with a spinel structure (JCPDS no. 22-1086). An additional peak around 26° resulted from the CNTs. The peaks are relatively broad in the XRD pattern, corresponding to the small grain size of the primary $CoFe_2O_4$ particles. This result is consistent with the following TEM observation. Thus the number of catalytic active sites would be increased, thereby improving the electrochemical activity of the air cathodes. Meanwhile, the $NiFe_2O_4$/CNTs show a similar XRD pattern (JCPDS no. 86-2267), also indicating a spinel structure.[28]

The TEM and HR-TEM images are shown in Fig. 2a–c. It can be found that most CNTs in the sample were well coated with small $CoFe_2O_4$ particles. Clear lattice fringes for $CoFe_2O_4$ are observed in Fig. 2c, suggesting the crystalline nature of the particles. The regular interplanar spacing of ~0.25 nm is ascribed to the (311) planes of $CoFe_2O_4$. The corresponding SAED pattern (shown in Fig. 2d) demonstrates the crystalline nature of $CoFe_2O_4$ particles. The diffraction rings are related to the (111), (220), (311), (400) and (440) planes of the spinel $CoFe_2O_4$. In order to further confirm the presence of $CoFe_2O_4$, element mapping was used to observe the distribution of $CoFe_2O_4$. As presented in Fig. 2e–i, the color points are due to the presence of the elements. It can be seen that Co, Fe and O in the sample are homogeneously distributed in the composite, indicating the $CoFe_2O_4$ particles are homogenously coated on the surface of the CNTs. Similarly, the morphology of $NiFe_2O_4$/CNTs shown in Fig. 3 revealed that the $NiFe_2O_4$ particles are well coated on the CNT surface. The uniform structure is beneficial to the fast migration of electrons between CNTs and

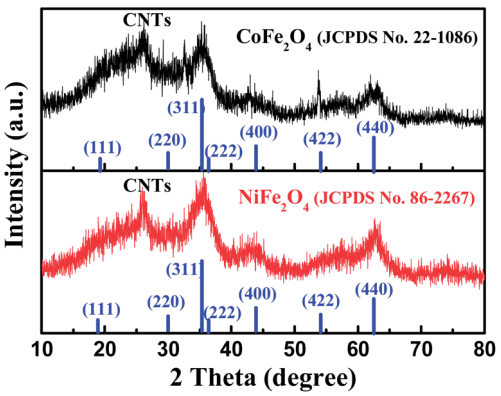

Fig. 1 XRD pattern of the MFe_2O_4/CNT (M = Co, Ni) composites.

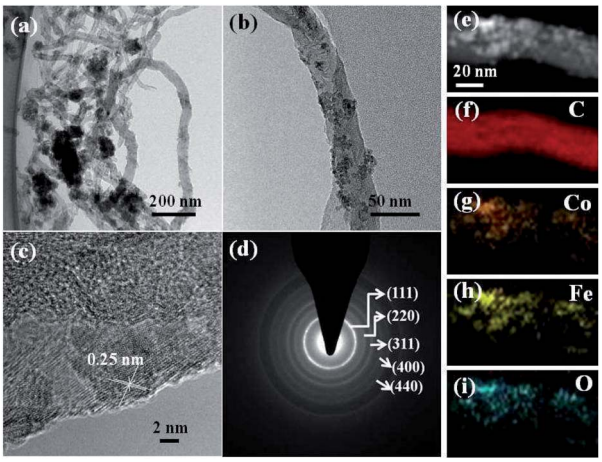

Fig. 2 (a)–(d) TEM, HR-TEM images and the corresponding SAED pattern of the $CoFe_2O_4$/CNTs; STEM image (c) and carbon (f), cobalt (g), iron (h) and oxygen (i) element mapping images of $CoFe_2O_4$/CNTs.

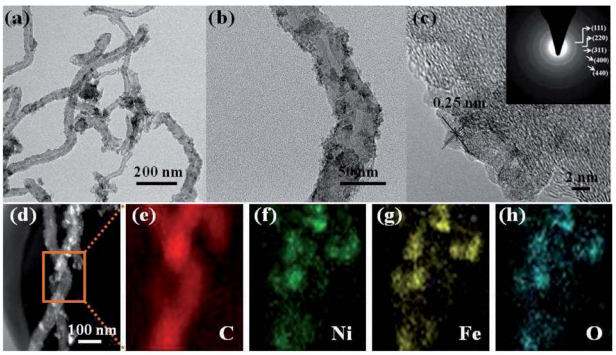

Fig. 3 (a)–(c) TEM, HR-TEM images and the corresponding selected area electron diffraction (SAED) pattern of the $NiFe_2O_4$/CNTs; STEM image (d) and carbon (e), nickel (f), iron (g) and oxygen (h) element mapping images of $NiFe_2O_4$/CNTs.

MFe_2O_4 (M = Co, Ni) particles, thereby improving electrocatalytic activity. Meanwhile, Fig. S1† shows the SEM and magnified SEM images of as-synthesized MFe_2O_4/CNTs (M = Co, Ni) materials. These two materials show homogeneous agglomerated and cross-linked morphology with a larger diameter in the range of 50–100 nm. Thus, the uniform coating layer of MFe_2O_4 (M = Co, Ni) materials can be observed. In addition, the EDS and XPS results shown in Fig. S2–S4† provide another proof of the elements of Co and Fe present in the composite of $CoFe_2O_4$/CNTs, and the elements of Ni and Fe present in the composite of $NiFe_2O_4$/CNTs. To further confirm the composition of MFe_2O_4 (M = Co, Ni) particles, Raman spectroscopy, as an alternative characterization method, was used to detect these two composites (Fig. S5†). Fig. S5† shows Raman spectra of the MFe_2O_4/CNTs (M = Co, Ni) between 100 and 1000 cm^{-1} using 543 nm excitation. According to the previous reports,[30,31] MFe_2O_4 (M = Co, Ni) crystallizes in a spinel structure of space group *Fd*-3*m* and group theoretical calculations results in five Raman active bands, namely, $A_{1g} + E_g + 3T_{2g}$. Furthermore, shoulder-like features at the lower wavenumber side of all the Raman active bands can be found, which revealed the spinel structure of MFe_2O_4 (M = Co, Ni). These Raman spectra of spinel MFe_2O_4 (M = Co, Ni) had been extensively reviewed by V. G. Sathe *et al.* and S. V. Narasimhan *et al.*[30,31] Meanwhile, the Raman spectra in this current work are in good agreement with those reported earlier.

To explore the application of the MFe_2O_4/CNTs (M = Co, Ni) as electrocatalysts in cathodes for LOBs, the cyclic voltammetry (CV) curves and discharge–charge (D–C) voltage profiles are shown in Fig. 4. Compared with the MFe_2O_4/CNT (M = Co, Ni) cathodes, a featureless CV curve of a pure KB cathode is observed in its OER process (shown in Fig. 4a). In the ORR scan, the KB cathode exhibits a slightly lower ORR onset potential in the first cycle and lower peak currents than both MFe_2O_4/CNT (M = Co, Ni) cathodes in the following cycles (shown in Fig. 4c and e). Accordingly, Fig. 4b shows that the discharge capacity of the KB cathode decreases from 3860 mA h g^{-1} at the 1st cycle to only 965 mA h g^{-1} at the 3rd cycle combined with a low charge capacity of 400 mA h g^{-1}, indicating that the D–C process for the KB cathode without MFe_2O_4/CNT (M = Co, Ni) electrocatalysts is almost irreversible. From Fig. 4c and e, the cathodes with MFe_2O_4/CNT (M = Co, Ni) electrocatalysts both exhibit obvious redox peaks, revealing that these two cathodes could enable the reaction "$2Li^+ + 2e^- + O_2 \leftrightarrow Li_2O_2$" to remain reversible during the ORR and OER processes. Compared with the $NiFe_2O_4$/CNT cathode shown in Fig. 4e, a higher ORR onset potential marked with a red box in Fig. 4c is observed for the $CoFe_2O_4$/CNT cathode. Meanwhile, the currents in the OER process which range from 3.0 to 3.5 V for the $CoFe_2O_4$/CNT cathode are larger than those of the $NiFe_2O_4$/CNT cathode. This result is attributed to the improved OER kinetics that facilitates more efficient decomposition of Li_2O_2. The initial three D–C curves for both

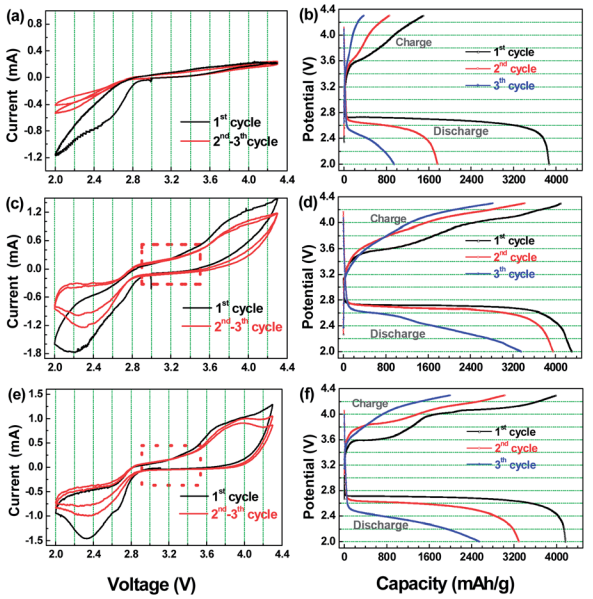

Fig. 4 Cyclic voltammetry curves and the first three discharge–charge curves between 2.0 and 4.3 V (*versus* Li/Li^+) of Li insertion/extraction into/from electrodes: (a and b) pure KB, (c and d) $CoFe_2O_4$/CNTs and (e and f) $NiFe_2O_4$/CNTs.

MFe_2O_4/CNT (M = Co, Ni) cathodes are depicted in Fig. 4d and f. The charge potential for the $CoFe_2O_4$/CNT cathode is ~3.85 V, lower than ~4.05 V of the $NiFe_2O_4$/CNT cathode. In addition, the remaining capacities for the $CoFe_2O_4$/CNT cathode are larger than that of the $NiFe_2O_4$/CNT cathode. Herein, the $CoFe_2O_4$/CNT cathode shows slightly more excellent performance than the $NiFe_2O_4$/CNT cathode. This phenomenon may be due to the high spin for Co^{2+} in an oxygen-atom ligand field associated with an easily forming stable ion pair with superoxide.[22,23] In brief, these findings indicate the effective catalytic activity of both MFe_2O_4/CNT (M = Co, Ni) composites in cathodes for LOBs.

To further get insights into the D–C process of LOBs with MFe_2O_4/CNT (M = Co, Ni) cathodes, the products after discharge and the subsequent charge process were analyzed by using SEM and XPS. For the pristine $CoFe_2O_4$/CNT cathode shown in Fig. 5a, the SEM analysis presents many $CoFe_2O_4$/CNT composites and KB nanospheres (the related SEM result is shown in Fig. S6†). Then the discharged products were deposited on the electrode (Fig. 5b) after the discharge process. Combined with the XPS results shown in Fig. 5d, the observed close-packed layer is believed to be Li_2O_2 intermingled with some Li_2CO_3. After charge, the Li_2O_2 products disappear and a relatively clean electrode is observed (Fig. 5c). However, some residual coating layer still remains, revealing minor undecomposition of Li_2CO_3.[32,33] Fig. 5d shows the absence of the Li_2CO_3 characteristic signal at 55.5 eV in the charge electrode, implying that the product was residual Li_2CO_3. The polarization resulted from residual Li_2CO_3 will increase their D–C over potentials, further leading to fading in their cycle performance.[34,35] As expected, similar SEM and XPS results for $NiFe_2O_4$/CNT electrodes can be obtained and is shown in Fig. 6. In addition, combined with the above discussion, the additional full XPS spectra and the C1s XPS spectra for both MFe_2O_4/CNT (M = Co, Ni) cathodes after discharge and the subsequent charge process are shown in Fig. S7 and 8.† As revealed in Fig. S8† for the C1s XPS spectra, the signal for C1s at ~292 eV for Li_2CO_3 can be found in both cathodes after discharge and recharge.

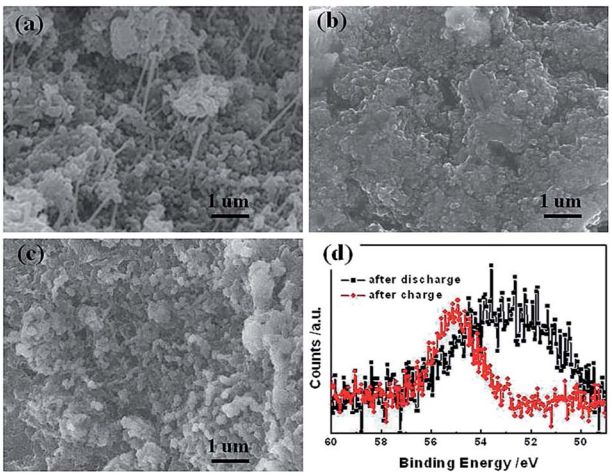

Fig. 5 SEM images of (a) the pristine $CoFe_2O_4$/CNT cathode, (b) the $CoFe_2O_4$/CNT cathode after discharge, (c) the $CoFe_2O_4$/CNT cathode after recharge, and (d) the corresponding XPS spectra for the $CoFe_2O_4$/CNT cathode after discharge and recharge.

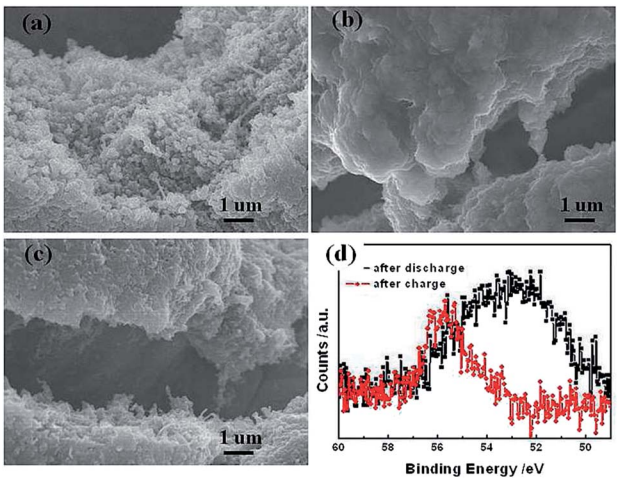

Fig. 6 SEM images of (a) the pristine $NiFe_2O_4$/CNT cathode, (b) the $NiFe_2O_4$/CNT cathode after discharge, (c) the $NiFe_2O_4$/CNT cathode after recharge, and (d) the corresponding XPS spectra for the $NiFe_2O_4$/CNT cathode after discharge and recharge.

It is well-known that the rate performance is an important evaluation index for the electrocatalysts in LOBs. Fig. 7 shows the discharge voltage and specific capacity decrease with increased current density for both MFe_2O_4/CNT (M = Co, Ni) cathodes. This phenomenon should be caused by significant chemical polarization at higher current densities.[36] Although both MFe_2O_4/CNT (M = Co, Ni) cathodes exhibit similar discharge capacities, the $CoFe_2O_4$/CNTs exhibit higher discharge potentials at different current densities than the $NiFe_2O_4$/CNTs (see the inset table shown in Fig. 7).

As shown in Fig. 8, the cycle stability of both MFe_2O_4/CNT (M = Co, Ni) cathodes is investigated with a restriction of the capacity to 800 mA h g^{-1} at a current density of 200 mA g^{-1}. The $CoFe_2O_4$/CNT cathode exhibits good capacity retention for 14

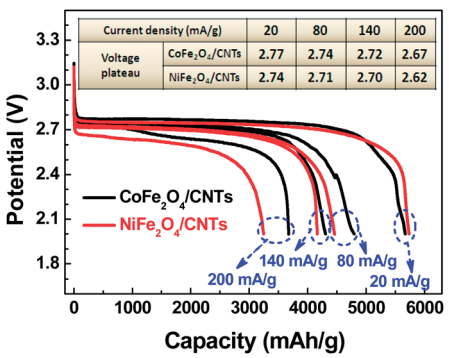

Fig. 7 The discharge curves at different current densities for both MFe_2O_4/CNT (M = Co, Ni) cathodes. The inset table shows the comparison between discharge voltage plateaus of $CoFe_2O_4$/CNT and $NiFe_2O_4$/CNT cathodes.

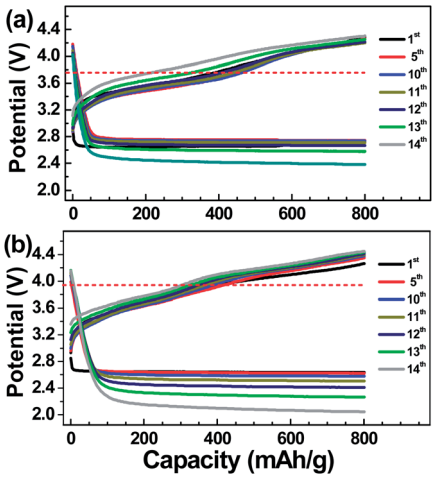

Fig. 8 Cycling performance of (a) the $CoFe_2O_4$/CNT cathode and (b) the $NiFe_2O_4$/CNT cathode at 200 mA g^{-1} with a restricting capacity of 800 mA h g^{-1}.

cycles. Although a decrease in the cutoff voltage is observed during cycling, the cutoff voltage of 2.4 V at the 13th cycle still remains acceptable. However, there is a significant drop in the cutoff voltage even from the 12th cycle for the $NiFe_2O_4$/CNT cathode. Furthermore, the charge potential for the $CoFe_2O_4$/CNT cathode is lower than that of the $NiFe_2O_4$/CNT cathode. These findings indicate slightly better catalytic activity for $CoFe_2O_4$/CNTs than that of $NiFe_2O_4$/CNTs. This result is consistent with the above conclusion.

As noted above, some residual products such as Li_2CO_3 may still remain on the electrode after the D–C process, resulting in capacity fading. For comparison, the restricting capacity for the $CoFe_2O_4$/CNT cathode was further reduced to 430 mA h g^{-1} at a current density of 200 mA g^{-1}. As shown in Fig. 9, the $CoFe_2O_4$/CNT cathode shows that the cutoff voltage does not change significantly after 30 cycles, being similar to those reported by Liu *et al.*[15] However, a significant drop in the cutoff voltage can be observed for the cathode after the 35th cycle. To further evaluate the CNT effect on the LOB performance, Fig. S9† compares the D–C characteristics of pure $CoFe_2O_4$ and $CoFe_2O_4$/CNT electrodes in LOBs at different current densities. It can be seen that the discharge voltage and specific capacity for both pure $CoFe_2O_4$ and $CoFe_2O_4$/CNT electrodes decrease with increased current density. Meanwhile, it is noticeable that the catalyst with the CNT support exhibits better capacity retention than pure $CoFe_2O_4$. As shown in Table S1,† the $CoFe_2O_4$/CNT electrode delivered a specific capacity of 3670 mA h g^{-1} at 200 mA g^{-1}, being much larger than 3045 mA h g^{-1} for pure $CoFe_2O_4$ without the CNT support. These results indicate that the presence of CNTs can slightly improve the charge transfer resistance of the electrode and may result in a low electrode interface polarization, which is considered to be responsible for the deterioration of the electrochemical performance.

Electrochemical impedance spectra (EIS) was used to further get insights into the deterioration mechanism of LOBs. Fig. 10 presents an EIS profile for LOBs after 35 cycles and the corresponding equivalent circuit.[37,38] In the circuit, the high frequency intercept of the semicircle on the real axis was reflected by an ohmic resistance (R_1), which includes ionic resistance from the separator paper and electrical resistance between the electrode and the current collector. The depressed semicircle at middle frequency was contributed by a parallel combination of charge-transfer resistance (R_2), corresponding to the kinetic reaction at the air electrode surface. The linear spike at low frequency could be described by a finite length Warburg element R_W. The fitting results indicate that the R_1 value of 25 Ω for the pristine electrode is smaller than 193 Ω after cycling, indicating the possible decomposition of the electrolyte by reaction with Li_2O_2 or KB especially at its defects as well as corrosion of CNTs.[32,35,36] Besides, the R_2 value of 190 Ω for the pristine electrode is obviously smaller than 650 Ω after cycling, suggesting that the capacity fading may be mainly from accumulation of the reaction products (such as Li_2CO_3).[35,36] Certainly, obtaining good electrochemical performance for LOBs is also dependent on other critical technological strategies such as fabricating cathodes with effective microstructures. At least, it can be concluded from this work that the spinel MFe_2O_4/CNT (M = Co, Ni) composites are promising electrocatalysts for achieving high-performance LOBs.

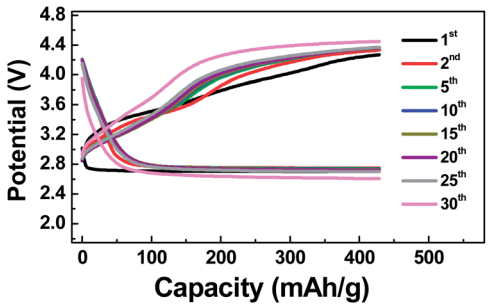

Fig. 9 Cycling performance of the $CoFe_2O_4$/CNT cathode at 200 mA g^{-1} with a restricting capacity of 430 mA h g^{-1}.

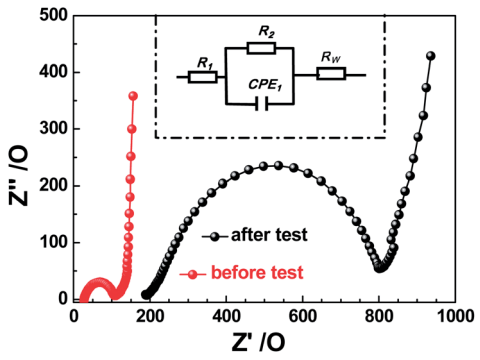

Fig. 10 The EIS profiles of the $CoFe_2O_4$/CNT cathode before and after long restricting cycling. The inset shows the corresponding equivalent circuit.

4. Conclusion

In conclusion, this work reports a fundamental study on developing ternary spinel MFe_2O_4/CNT (M = Co, Ni) electrocatalysts that are prepared *via* a simple hydrothermal method. The electrochemical performance of LOBs, including round trip efficiency, can be much improved by using these two electrocatalysts. The good performance can be attributed to the excellent catalytic activity of highly dispersed MFe_2O_4 (M = Co, Ni) nanoparticles and facile electron transport by supporting CNTs. The present investigation proves that the ternary spinel MFe_2O_4/CNTs (M = Co, Ni) are promising cathode electrocatalysts for LOBs.

Acknowledgements

We acknowledge the financial support from the Natural Science Foundation of China (no. 21203025, 91127020), the Strategic Priority Research Program of the Chinese Academy of Sciences (Grant no. XDA09010400), and the National Key Project on Basic Research (Grant no. 2011CB935904).

Notes and references

1 Z. Jian, P. Liu, F. Li, P. He, X. Guo, M. Chen and H. Zhou, *Angew. Chem., Int. Ed.*, 2014, **53**, 442–446.
2 T. H. Yoon and Y. J. Park, *J. Power Sources*, 2013, **244**, 344–353.
3 K. Huang, Y. Li and Y. Xing, *Electrochim. Acta*, 2013, **103**, 44–49.
4 H. Nie, H. Zhang, Y. Zhang, T. Liu, J. Li and Q. Lai, *Nanoscale*, 2013, **5**, 8484–8487.
5 Y. Yang, Q. Sun, Y.-S. Li, H. Li and Z.-W. Fu, *J. Power Sources*, 2013, **223**, 312–318.
6 H. Minowa, M. Hayashi, K. Hayashi, R. Kobayashi and K. Takahashi, *J. Power Sources*, 2013, **244**, 17–22.
7 C. Kok Poh, S. Hua Lim, Z. Tian, L. Lai, Y. Ping Feng, Z. Shen and J. Lin, *Nano Energy*, 2013, **2**, 28–39.
8 Y. Lei, J. Lu, X. Luo, T. Wu, P. Du, X. Zhang, Y. Ren, J. Wen, D. J. Miller, J. T. Miller, Y. K. Sun, J. W. Elam and K. Amine, *Nano Lett.*, 2013, **13**, 4182–4189.
9 D. Su, H.-S. Kim, W.-S. Kim and G. Wang, *J. Power Sources*, 2013, **244**, 488–493.
10 H. Yang, J. Zhang, S. Kumar, H. Zhang, R. Yang, J. Fang and S. Zou, *Electrochem. Commun.*, 2009, **11**, 2278–2281.
11 R. Mi, H. Liu, H. Wang, K.-W. Wong, J. Mei, Y. Chen, W.-M. Lau and H. Yan, *Carbon*, 2014, **67**, 744–752.
12 J. Park, Y.-S. Jun, W.-r. Lee, J. A. Gerbec, K. A. See and G. D. Stucky, *Chem. Mater.*, 2013, **25**, 3779–3781.
13 J. L. Shui, N. K. Karan, M. Balasubramanian, S. Y. Li and D. J. Liu, *J. Am. Chem. Soc.*, 2012, **134**, 16654–16661.
14 G. Zhao, J. Lv, Z. Xu, L. Zhang and K. Sun, *J. Power Sources*, 2014, **248**, 1270–1274.
15 T. F. Hung, S. G. Mohamed, C. C. Shen, Y. Q. Tsai, W. S. Chang and R. S. Liu, *Nanoscale*, 2013, **5**, 12115–12119.
16 S. Ma, L. Sun, L. Cong, X. Gao, C. Yao, X. Guo, L. Tai, P. Mei, Y. Zeng, H. Xie and R. Wang, *J. Phys. Chem. C*, 2013, **117**, 25890–25897.
17 W. H. Ryu, T. H. Yoon, S. H. Song, S. Jeon, Y. J. Park and I. D. Kim, *Nano Lett.*, 2013, **13**, 4190–4197.
18 H. Wang, Y. Yang, Y. Liang, G. Zheng, Y. Li, Y. Cui and H. Dai, *Energy Environ. Sci.*, 2012, **5**, 7931.
19 Y. Qin, J. Lu, P. Du, Z. Chen, Y. Ren, T. Wu, J. T. Miller, J. Wen, D. J. Miller, Z. Zhang and K. Amine, *Energy Environ. Sci.*, 2013, **6**, 519.
20 A. Débart, J. Bao, G. Armstrong and P. G. Bruce, *J. Power Sources*, 2007, **174**, 1177–1182.
21 W. Yang, J. Salim, C. Ma, Z. Ma, C. Sun, J. Li, L. Chen and Y. Kim, *Electrochem. Commun.*, 2013, **28**, 13–16.
22 J. Xu, P. Gao and T. S. Zhao, *Energy Environ. Sci.*, 2012, **5**, 5333.
23 M. J. Trahan, Q. Jia, S. Mukerjee, E. J. Plichta, M. A. Hendrickson and K. M. Abraham, *J. Electrochem. Soc.*, 2013, **160**, A1577–A1586.
24 Y. Liang, Y. Li, H. Wang, J. Zhou, J. Wang, T. Regier and H. Dai, *Nat. Mater.*, 2011, **10**, 780–786.
25 W. M. Liu, T. T. Gao, Y. Yang, Q. Sun and Z. W. Fu, *Phys. Chem. Chem. Phys.*, 2013, **15**, 15806–15810.
26 D. U. Lee, B. J. Kim and Z. Chen, *J. Mater. Chem. A*, 2013, **1**, 4754.
27 H. W. Park, D. U. Lee, L. F. Nazar and Z. Chen, *J. Electrochem. Soc.*, 2012, **160**, A344–A350.
28 Y. Zhao, J. Li, Y. Ding and L. Guan, *J. Mater. Chem.*, 2011, **21**, 19101.
29 J. Li, N. Wang, Y. Zhao, Y. Ding and L. Guan, *Electrochem. Commun.*, 2011, **13**, 698–700.
30 A. Ahlawat and V. G. Sathe, *J. Raman Spectrosc.*, 2011, **42**, 1087–1094.
31 P. Chandramohan, M. P. Srinivasan, S. Velmurugan and S. V. Narasimhan, *J. Solid State Chem.*, 2011, **184**, 89–96.
32 M. M. Ottakam Thotiyl, S. A. Freunberger, Z. Peng and P. G. Bruce, *J. Am. Chem. Soc.*, 2013, **135**, 494–500.
33 S. A. Freunberger, Y. Chen, N. E. Drewett, L. J. Hardwick, F. Bardé and P. G. Bruce, *Angew. Chem., Int. Ed.*, 2011, **50**, 8609–8613.
34 Y. Zhang, H. Zhang, J. Li, M. Wang, H. Nie and F. Zhang, *J. Power Sources*, 2013, **240**, 390–396.
35 B. D. McCloskey, A. Speidel, R. Scheffler, D. C. Miller, V. Viswanathan, J. S. Hummelshøj, J. K. Nørskov and A. C. Luntz, *J. Phys. Chem. Lett.*, 2012, **3**, 997–1001.
36 X. Lin, L. Zhou, T. Huang and A. Yu, *J. Mater. Chem. A*, 2013, **1**, 1239.
37 H. Kitaura and H. Zhou, *Adv. Energy Mater.*, 2012, **2**, 889–894.
38 P. Kichambare, J. Kumar, S. Rodrigues and B. Kumar, *J. Power Sources*, 2011, **196**, 3310–3316.

